Sensors and Materials, Vol. 34, No. 5 (2022) 1629–1638
MYU Tokyo

S & M 2915

Analysis of Adhesion Strength between Silver Film and Substrate in Plain Silver Surface Plasmon Resonance Imaging Sensor

Zhiyou Wang,[1*] Ye Wang,[2] Maojin Wang,[1] and Qinfang Zheng[2**]

[1]School of Electronic Communication and Electrical Engineering, Changsha University,
98th Hongshan Rd, Changsha 410022, China
[2]Key Laboratory of Dong Medical Research of Hunan Province, Hunan University of Medicine,
492nd Jinxi South Rd, Huaihua 418000, China

(Received December 6, 2021; accepted March 9, 2022)

Keywords: plain silver SPRi sensor, gold adhesion-enhancing layer, indentation-induced film breaking

Recently, a plain silver surface plasmon resonance imaging (SPRi) sensor with a gold adhesion-enhancing layer has been studied extensively because of its desirable sensitivity and durability. To study the effect of the gold adhesion-enhancing layer on the durability of the sensor, we studied the adhesion strength between the silver film and the substrate. In a cross-sectional analysis, we observed the spatial elemental distribution of the sensor and found clear chromium–gold and gold–silver interfaces under transmission electron microscopy (TEM). By the indentation-inducing film method, we measured the critical load and depth of the silver film breaking. We also tested the working and shelf lives of the sensor with different thicknesses of the adhesion-enhancing layer. Testing results showed that the adhesion-enhancing layer thickness was related to the shelf life of the sensor. Results of the above studies showed that the gold adhesion-enhancing layer improved the adhesion strength of the silver film and the durability of the plain silver SPRi sensor.

1. Introduction

Featuring label-free and real-time measurements, surface plasmon resonance imaging (SPRi) sensors have been extensively used as high-throughput tools in different applications, such as analytical chemistry, food safety, and drug development.[1–4] Among the currently available SPRi active metals, gold is most used because of its pronounced chemical inertia and ease of fabrication, although its SPRi sensitivity is limited.[5,6] By contrast, SPRi structures based on silver films are more attractive owing to their much higher sensitivity performance; however, the adhesion strength of the film is hindered by the chemical activity of the silver material.[7] Tremendous efforts of researchers have been focused on cover layers, e.g., organic, oxide, and inertia metal, on top of the silver film against contacting chemical reagents, which are considered to improve the adhesion strength of the silver film within 120 min.[8–10] On the basis of the reported wettability of silver on gold and peeling-off phenomena of a silver film from a

*Corresponding author: e-mail: zywang@ccsu.edu.cn
**Corresponding author: e-mail: zqfzqf2@126.com
https://doi.org/10.18494/SAM3802

ISSN 0914-4935
https://myukk.org/

chromium substrate adhesion layer, we reported a plain silver SPRi sensor by adding a 2 nm gold adhesion-enhancing layer between the silver film and the chromium layer.[11,12] With the silver film covered by an 11-mercaptoundecanoic acid self-assembled monolayer (SAM), the sensor can have a working life of more than 10 h in chemical environments and a shelf life as long as 105 days. The reported working life promotion proves that the insertion of the gold layer improves the durability of the silver film.[13,14]

To determine the effect of the gold adhesion-enhancing layer on the durability of the silver film in the sensor, the spatial elemental distribution within the sensor structure and the exact adhesion strength between the silver film and the substrate need to be studied. According to previous studies, the 2-nm-thick gold adhesion-enhancing layer can be modeled as an island film with an area coverage of around 50%.[15] In this type of film, randomly distributed vacancies, lattice defects, and grain boundaries can considerably increase the diffusion speed of all the elements adjacent to the gold–silver interface. During the diffusion, silver atoms across the interface can be trapped by gold grains and form gold–silver bonds, which are much stronger than silver–silver bonds, and can improve the adhesion strength of the silver film in the sensor.[16] By contrast, fewer gold atoms can diffuse across the gold–silver interface since the gold–silver bond is weaker than the gold–gold bond. Thus, research on the existence of the gold–silver interface and silver atom diffusion in the gold layer is necessary for studying the effect of the gold layer on the adhesion enhancement of the silver film.

Adhesion strength measurement methods of the silver film can be mainly categorized into two types: adhesion cross-cut testing and indentation-induced film breaking.[17] In the adhesion cross-cut testing methods, the film surface is cut into hundreds of grids and peeled off by different types of tape. The ratio between the number of peeled-off grids and that of all grids, i.e., peeled-off ratio, is calculated to estimate the adhesion strength qualitatively.[18] In indentation-induced film breaking methods, a load force is added onto probes to penetrate into the film. The measured penetration depth and load force of film breaking are defined as the critical load depth and critical load force, respectively.[19] The adhesion of the film is stronger if the peeled-off ratio is lower or the critical load force is higher. With smaller probe sizes and more options of probe types among the two types of method, the indentation-induced film breaking method has been widely used in the film adhesion strength study of micro- and nanostructures.[20–24] However, the two types of method have not yet been tried on the plain silver SPRi sensor.

Note that the plain silver SPRi sensor has been reported to demonstrate long-term durability, intrinsic physical properties, and desirable silver film adhesion among different types of silver-film-based SPRi sensor.[11–14] Studying the effects of the gold adhesion-enhancing layer on the durability and adhesion of the sensor can help improve the stability and applicability of the silver material in different types of sensor. In this work, we analyzed the spatial structure and measured the adhesion strength of the plain silver SPRi sensor. Firstly, we fabricated the sensor and characterized its surface roughness at different gold and silver thicknesses by atomic force microscopy (AFM). Then, we prepared a cross-sectional example of the sensor using a focused ion beam (FIB) for spatial elemental distribution analysis. Under transmission electron microscopy (TEM), a clear gold–silver interface and silver atom diffusion into the gold layer can be observed in the sensor. In the following adhesion cross-cut testing method, the center area of

the silver film was cut into numerous grids using a cross-cutter and peeled off with Scotch tape. No peel-off phenomenon was observed in the plain silver SPRi sensor under optical microscopy, whereas the phenomenon can be observed in all the grids of a silver SPRi sensor without the gold adhesion-enhancing layer. To measure the critical load force and load depth of the silver film in the plain silver SPRi sensor, a Berkovich probe was used in the indentation-induced film breaking method. When the area of the probe is considered, the measured critical load force of the film breaking was around 1.26 mN, which was comparable to that of the silver film immobilized on 3-mercaptopropyltrimethoxysilane (MTPMS) by a silver–sulfur bond.[24] To further evaluate the effect of the gold adhesion-enhancing layer on the durability of the sensor, working and shelf lives were recorded at different thicknesses. The above results indicate that the insertion of the gold adhesion layer increases the adhesion strength of the silver film and the durability of the plain silver SPRi sensor. Further optimization of the gold adhesion layer thickness can help spread the usage of the sensor.

2. Materials and Methods

2.1 Materials

BK7 Schott glass (75 mm × 25 mm), chromium, gold, silver, poly(ethylene glycol) 2-mercaptoethyl ether acetic acid (CAS no. 165729-81-7), phosphate-buffered saline (PBS), phosphorus acid, and sodium hydroxide were purchased according to our previous work.[11,12]

2.2 Methods

The plain silver SPRi sensor and a silver SPRi sensor composed of chromium, silver (50 nm), and SAM layers, i.e., the reference sensor, were fabricated according to our previous work.[11,12] AFM (Dimension icon, Veeco, Germany) was employed to characterize the surface morphology of the silver film. In spatial elemental distribution analysis, cross-sectional samples of the sensor were prepared by FEI Helios NanoLab 600i DualBeam FIB/SEM for TEM observations. At an early stage of the sample cutting, the acceleration voltage of 30 kV was applied to the ion gun, and then the acceleration voltage was gradually reduced to 5 kV. Finally, the acceleration voltage of 2 kV was applied to the ion gun for sample cutting. Scanning TEM experiments were performed on a JEOL JEM-ARM200F transmission electron microscope with double spherical aberration correctors for both the condenser and objective lenses, and a cold field emission gun that was operated at an acceleration voltage of 200 kV. The high-angle annular dark-field (HAADF), annular bright-field (ABF), and energy-dispersive X-ray (EDX) mapping techniques were applied to obtain information on the microstructure and elemental distribution. The experimental convergence semi-angle of the incident electron beam was about 22 mrad. The HAADF and ABF images were acquired at acceptance angles of 70−150 and 10−20 mrad, respectively. The EDX mapping images were acquired and processed with the software supplied by the JEOL manufacturer.

In the adhesion cross-cut testing method, the center area of the silver film in both the plain silver SPRi and reference sensors was cut into 100 1 mm × 1 mm grids and peeled off with

Scotch tape under an Axiocam 105 color optical microscope (Carl Zeiss AG) separately. In the indentation-induced film breaking method, the critical load force and load depth of the silver film in the plain silver SPRi sensor were measured using a Hysitron TI 950 triboindenter (Bruker Co.) with a Berkovich probe.

The working and shelf lives of the sensor were recorded on an HT arrayer (Plexera Co.) with a time resolution of 1 s according to our previous work.[11,12] In the working life test, 25 cycles of different reagents, i.e., PBS (pH = 7.4), PBS plus 1 %wt glycerol, phosphorous acid (pH = 2), and sodium hydroxide solution (pH = 13), were injected into the sensor. The average sensitivity of the sensor was calculated through the surface in each circle. In the shelf life test, the sensor was stored under dark and dry conditions at 4 ℃ for more than 100 days. The depth of the SPRi spectrum was recorded every three days, and the day corresponding to a depth drop of more than 3% determines the shelf life.

3. Results and Discussion

The surface morphology of the plain silver SPRi sensor was observed by AFM according to our previous work.[25] The surface roughness was distributed between 0.5 and 0.55 nm at different gold and silver layer thicknesses (Fig. 1), which proves that the effect of the gold and silver layer thicknesses on surface morphology can be ignored for further adhesion analysis.

When the thicknesses of the gold adhesion-enhancing layer and silver film are 2 and 50 nm, respectively, the cross section of the sensor structure was observed by TEM as in Fig. 2. In the figure, although the atom diameters of gold and silver are comparable, the atomic weight of gold is larger than that of silver. Thus, the gold layer can be observed as the black layer from the silver film. Because the gold layer is too thin to form a continuous film, it is more likely a discontinuous island structure in Fig. 2(b). From the cross-sectional observation of the sensor structure (Fig. 2) and quantitative measurements of the spatial elemental distribution (Fig. 3), we can find very

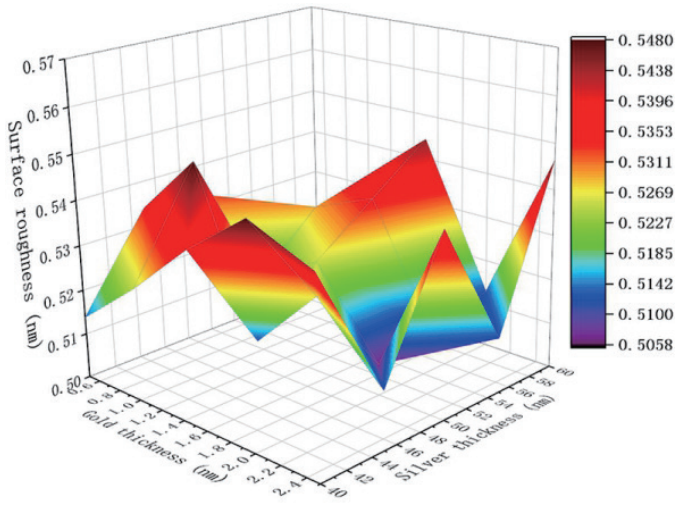

Fig. 1. (Color online) Sensor surface roughnesses at different gold and silver thicknesses.

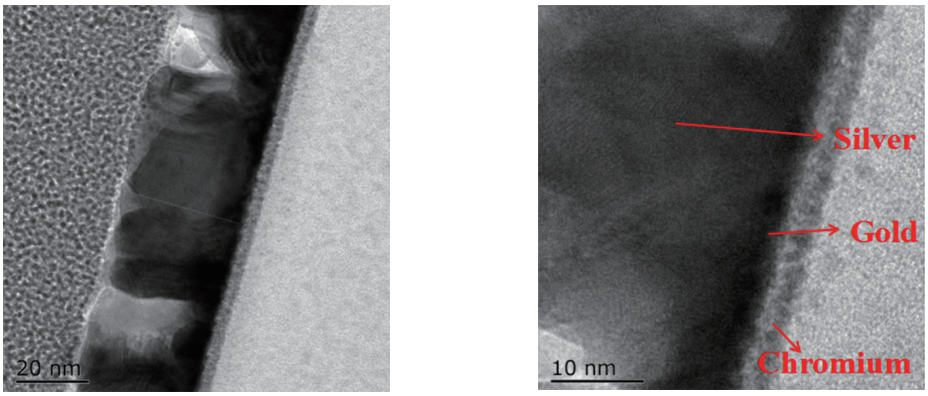

(a) (b)

Fig. 2. (Color online) Cross-sectional images of the sensor obtained by TEM: (a) global view of the spatial structure and (b) local view of gold–chromium and gold–silver boundaries.

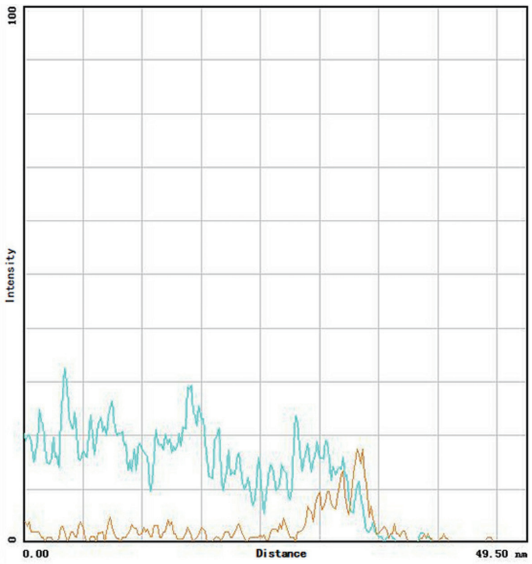

Fig. 3. (Color online) Spatial elemental distributions of gold (brown) and silver (cyan) vertical to the gold–silver boundary in the sensor.

clear gold–silver interfaces. At the side of the silver film, the diffusion of the gold element is limited by the total amount of gold, which helps maintain gold atoms in the gold layer for the formation of gold–silver bonds. By contrast, because the diffusion of the silver element can be quite fast in a 2-nm-thick gold layer, a large portion of the silver elemental distribution can be seen throughout the gold layer. Thus, the function of the adhesion-enhancing layer can be explained as providing a gold–silver elemental ratio sufficient for building a large number of gold–silver bonds, which is considered to improve the adhesion strength of the silver film in the sensor.[15,16]

In the following adhesion strength measurements, the gold and silver layer thicknesses in the sensor structure were 1.5 and 50 nm, respectively. In the adhesion cross-cut testing method, the

integrity of both the plain silver SPRi and reference sensors was observed under the optical microscope after the peeling-off operations. In the plain silver SPRi sensor, no peel-off phenomenon was observed in both the global and local views of all the grids as in Fig. 4. By contrast, the peel-off phenomenon can be found in all the grids of the reference sensor as in Fig. 5. Besides, different colors rather than the intrinsic luster of silver can be observed on the reference sensor, which can be explained as the oxidation of the silver film caused by a large area of exposure to oxygen after the peeling-off operation. Results of the comparative study showed that the gold adhesion-enhancing layer in the plain silver SPRi sensor helps improve the adhesion of the silver film.

In the indentation-induced film breaking method, the adhesion strength of the silver film in the plain silver SPRi sensor was quantitatively analyzed. Since silver and gold are soft materials with excellent ductility and malleability,[22] film breaking force and thickness can only be measured under slow loading conditions.[23,24] In the measurements, the relationship between the load force F and the time t is shown as

$$F(mN) = \begin{cases} 1.8 \cdot t, & t < 5, \\ 9, & 5 \le t \le 7, \\ 9 - 1.8 \cdot (t - 7), & 7 < t \le 12. \end{cases} \tag{1}$$

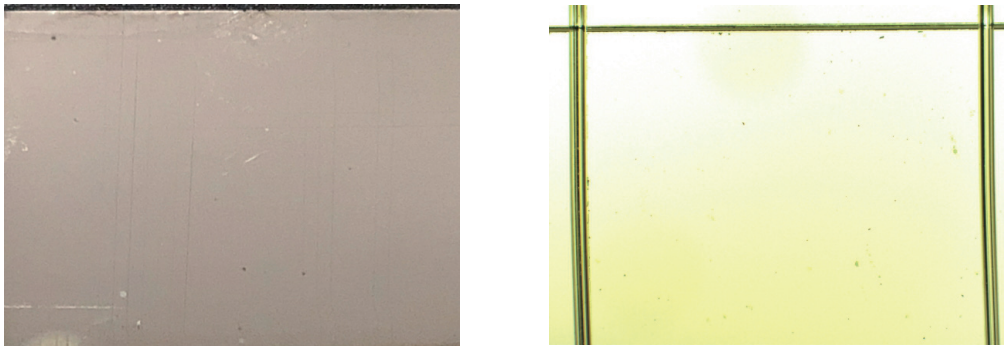

(a) (b)

Fig. 4. (Color online) (a) Global and (b) local views of plain silver SPRi sensor after the peeling-off operation.

Fig. 5. (Color online) Global view of the reference sensor after the peeling-off operation.

Aside from the physical properties of the metal materials, the total thickness of the gold and silver layers is only around 60 nm, which is too small to obtain the load depth data in a single film breaking operation. In this case, we set the maximal value of the load depth as 300 nm and collect continuous results of mechanical properties with reasonable repeatability in observation. To measure the critical load force and load depth of film breaking, both hardness and modulus data were collected (Fig. 6). According to the curvature of the measured hardness and modulus versus depth, the collected data can be divided into two zones by the dashed line in the figure: film-dominated zone and substrate-dominated zone. When the load depth was small, most of the probe penetrated the silver film, which is softer than the substrate. When the probe went deep, it broke the silver film and contacted with the glass substrate. Thus, the measured hardness and modulus were noncontinuous in the figure. Although the hardness of the glass substrate is larger than that of the silver film, the modulus of the substrate is smaller and more continuous than that of the film. Thus, the critical point between the two zones, i.e., the dashed line in the figures, can be determined as the exact interface between the film and the substrate, where we can measure the critical load depth and load force of the silver film breaking. From Fig. 6, the critical load force and load depth of the silver film breaking were around 1.26 mN and 70 nm, respectively. The deviation between the measured critical depth and the designed silver film thickness can be explained as thickness control deviation during fabrication and substrate flatness defects. After the measurements of the critical load depth and load force, the film profile was examined under the triboindenter as the post image in our previous work, where the shape of the Berkovich probe can be observed clearly.[25] This result further proves that the silver film breaking did occur during the indentation measurements when we measured the critical load force and load depth.

Note that the area of the probe in our previous work was around 2 μm^2, and the pressure caused by the critical load force can be calculated as 0.628 GPa.[25] In Ma and Clarke's work, the pressure caused by the average load at failure of a 90 nm silver film directly evaporated on rocksalt and collodion substrates was 0.23 GPa when the area of the Berkovich probe used was

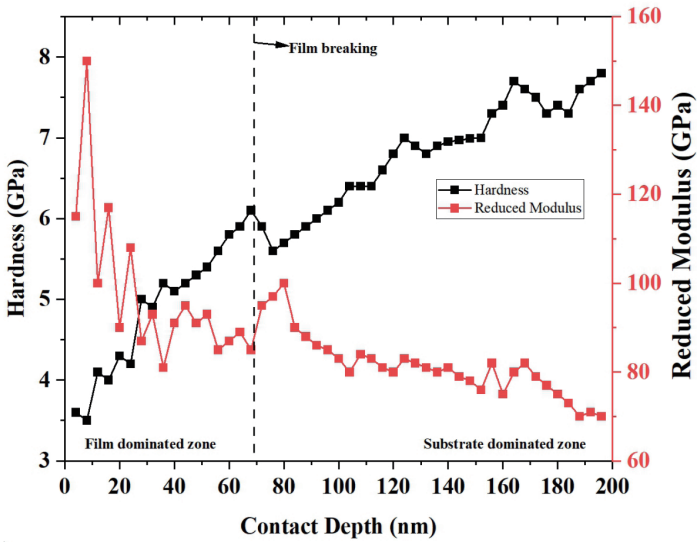

Fig. 6. (Color online) Critical load force and load depth measurements of the sensor.

around 2 μm^2.[23] In Kawamura *et al.*'s work, the pressure caused by the critical load force for a 60-nm-thick silver film immobilized on MTPMS by silver–sulfur bonds was 1.38 GPa when the area of the microscratch stylus was around 12 μm^2.[24] According to Beegan *et al.*'s work, for the same sample, the pressure measured in the microscratch test was around twofold that measured by the nanoindentation method.[26] Thus, with the aid of the gold adhesion-enhancing layer, the critical load force in film breaking in the plain silver SPRi sensor was comparable to those in previous works.

On the basis of the above measured physical stability improvement introduced by the gold adhesion-enhancing layer, we further analyzed the effect of its thickness on the durability of the sensor as below. We already reported that the gold thickness of 2 nm was sufficient for desirable working and shelf lives; thus, we tried smaller thicknesses, i.e., 1.0 and 1.5 nm, in this work.[11,12] The sensitivities of the sensors at the different gold thicknesses were calculated in the 25 cycles of reagent injections as in our previous work (Fig. 7). When the gold thickness was 1.0 nm, the average sensitivity remained around 8456.38 %/refractive index unit (RIU). When the gold thickness was 1.5 nm, the average sensitivity remained around 8378.54 %/RIU during the injections. The spatial sensitivity variation of the above calculations was less than 3%, which proves that changing the thickness of the gold adhesion-enhancing layer does not affect the durability of the sensor in reagents.

In the test of shelf life, the average surface plasmon resonance (SPR) curve depth of the sensor slide remained around 12 and 11% in Fig. 8 when the gold thicknesses were 1.5 and 1.0 nm, respectively. After 111 days of testing, the curve depth deteriorated more than 3% when the gold thickness changed, which was almost identical to our previously reported shelf life. Instead of the durability of the sensor slide, the different gold thicknesses can introduce variation in both the sensitivity and SPR curve depth in Figs. 7 and 8, respectively. The insertion of the gold adhesion-enhancing layer did not reportedly change the intrinsic SPRi properties of the silver film; however, the spatial electromagnetic field distribution inside the sensor structure changes

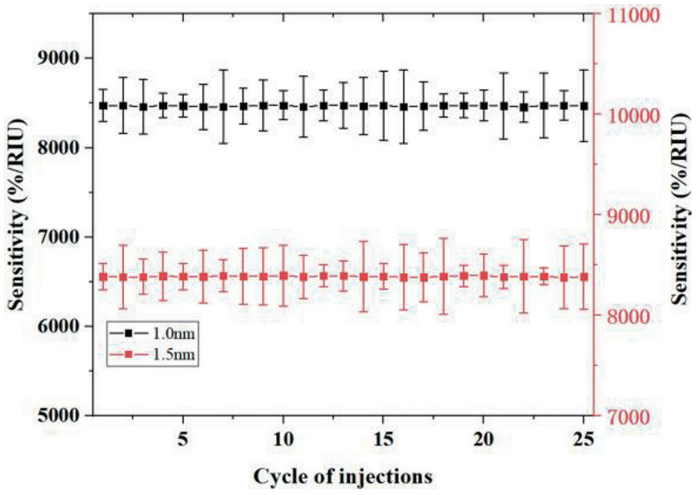

Fig. 7. (Color online) Sensitivity variation of the sensors at different gold thicknesses during 25 cycles of reagent injections.

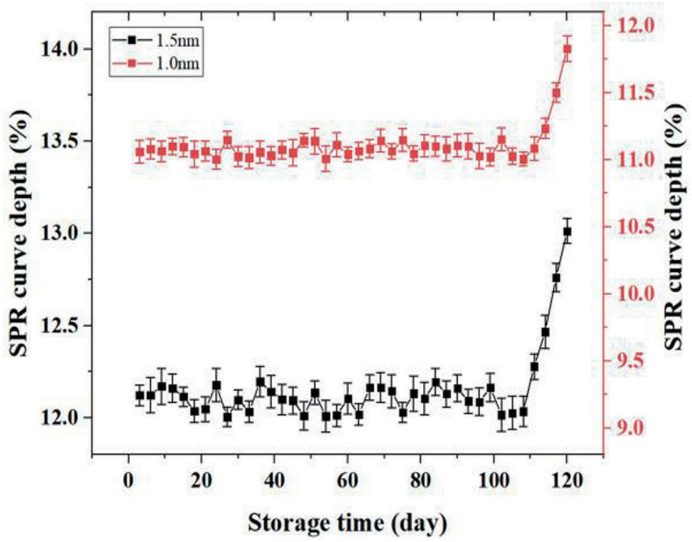

Fig. 8. (Color online) Shelf life test of sensors at different gold thicknesses.

when the gold thickness varies.[27] To sum up, the optimization of the thickness of the gold adhesion-enhancing layer can not only help improve the adhesion strength of the silver film and the durability of the plain silver SPRi sensor, but also promote the SPR curve depth and sensitivity.

4. Conclusions

In this work, we studied the phenomenon of durability improvement introduced by a gold adhesion-enhancing layer in a plain silver SPRi sensor. The studies include surface morphology analysis, the cross-sectional observation of spatial elemental distribution, the measurement of silver film adhesion strength, and the optimization of the gold thickness in terms of sensitivity and durability. All the results showed that the gold adhesion-enhancing layer was an island film in the structure, which markedly changed the spatial elemental distribution of the sensor. Both the island film structure and elemental distribution can provide sufficient conditions for establishing numerous strong gold–silver bonds. When compared with the silver sensor without the gold layer in the cross-cut testing method, the gold adhesion-enhancing layer improves the adhesion strength of the silver film in the plain silver SPRi sensor. In the following indentation-induced film breaking method, the critical load force and load depth of the silver film breaking were measured as around 1.26 mN and 70 nm, respectively. In the test of the working and shelf lives of the plain silver SPRi sensor, changing the thickness of the gold adhesion-enhancing layer can help optimize the SPR curve depth and sensitivity. The studies reported in this work can be very helpful in research on principles of improving adhesion strength, durability, and sensitivity of silver films, and can also provide sufficient support for expanding the usage of silver materials in chemical reagents.

Acknowledgments

This work was supported by the National Natural Science Foundation of China (Grant No. 61905027), the Key Research and Development Program of Hunan Province (Grant No. 2020SK2111), and the Program of the Educational Commission of Hunan Province (Grant No. 20B418).

References

1 J. Homola: Chem. Rev. **108** (2008) 462. https://doi.org/10.1021/cr068107d
2 C. L. Wong and M. Olivo: Plasmonics **9** (2014) 809. https://doi.org/10.1007/s11468-013-9662-3
3 C. Liu, F. Hu, W. Yang, J. Xu, and Y. Chen: Trends Anal. Chem. **97** (2017) 354. https://doi.org/10.1016/j.trac.2017.10.001
4 F. R. Castiello and M. Tabrizian: Anal. Chem. **90** (2018) 3132. https://doi.org/10.1021/acs.analchem.7b04288
5 S. Zhao, M. Yang, W. Zhou, B. Zhang, Z. Cheng, J. Huang, M. Zhang, Z. Wang, R. Wang, Z. Chen, J. Zhu, and H. Li: Proc. Natl. Acad. Sci. U. S. A. **114** (2017) E7245. https://doi.org/10.1073/pnas.1704155114
6 I. Miyazaki, S. Simizu, H. Okumura, S. Takagi, and H. Osada: Nat. Chem. Biol. **6** (2010) 667. https://doi.org/10.1038/nchembio.423
7 L. Xia, S. Yin, H. Gao, Q. Deng, and C. Du: Plasmonics **6** (2011) 245. https://doi.org/10.1007/s11468-010-9195-y
8 Y. Chen, R. S. Zheng, D. G. Zhang, Y. H. Lu, P. Wang, H. Ming, Z. F. Luo, and Q. Kan: Appl. Opt. **50** (2011) 387. https://doi.org/10.1364/AO.50.000387
9 C. T. Li, K. C. Lo, and H. Y. Chang: Biosens. Bioelectron. **36** (2012) 192. https://doi.org/10.1016/j.bios.2012.04.016
10 G. Manickam, R. Gandhiraman, R. K. Vijayaraghavan, L. Kerr, C. Doyle, D. E. Williams, and S. Daniels: Analyst **137** (2012) 5265. https://doi.org/10.1039/c2an35826c
11 Z. Cheng, Z. Wang, D. E. Gillespie, C. Lausted, M. Yang, Z. Zheng, and J. Zhu: Anal. Chem. **87** (2015) 1466. https://doi.org/10.1021/ac504110t
12 Z. Wang, Z. Zheng, K. Wang, Y. Su, L. Liu, L. Song, Y. Bian, R. Hou, S. Li, and J. Zhu: Anal. Chem. **86** (2014) 1430. https://doi.org/10.1021/ac402126k
13 G. Wang, C. Wang, R. Yang, W. Liu, and S. Sun: Sensors **17** (2017) 2777. https://doi.org/10.3390/s17122777
14 G. A. Lopez-Munoz, M. C. Estevez, M. Vazquez-Garcia, M. Berenguel-Alonso, J. Alonso-Chamarro, A. Homs-Corbera, and L. M. Lechuga: J. Biophotonics **11** (2018) e201800043. https://doi.org/10.1002/jbio.201800043
15 Y. Jiang, S. Pillai, and M. A. Green: J. Appl. Phys. **120** (2016) 233109. https://doi.org/10.1063/1.4972471
16 M. Loncaric, J. Sancho-Parramon, H. Zorc, S. Šegota, P. Dubček, and S. Bernstorff: Thin Sol. Films **591** (2015) 204. https://doi.org/10.1016/j.tsf.2015.04.031
17 T. Ohmura: Mater. Trans. **62** (2021) 563. https://doi.org/10.2320/matertrans.MT-M2020371
18 E. B. T. Walch and C. Roos: Int. J. Appl. Glas. Sci. **11** (2020) 195. https://doi.org/10.1111/ijag.13875
19 M. Ouchabane, C. Dublanche-Tixier, and D. Dergham: J. Appl. Phys. **122** (2017) 175103. https://doi.org/10.1063/1.5009756
20 E. Rossi, M. Sebastian, R. Gigliotti, and M. D'Amato: Int. J. Archit. Heritage **15** (2021) 79. https://doi.org/10.1080/15583058.2020.1737986
21 R. Han and J. J. Chen: J. Mater. Res. **36** (2021) 1762. https://doi.org/10.1557/s43578-021-00206-5
22 W. Wen, A. A. Becker, and W. Sun: J. Mat. Sci. **52** (2017) 12553. https://doi.org/10.1007/s10853-017-1348-3
23 Q. Ma and D. R. Clarke: J. Mater. Res. **10** (1995) 853. https://doi.org/10.1557/JMR.1995.0853
24 M. Kawamura, T. Fudei, and Y. Abe: Proc. 2013 15th Int. Conf. Thin Films (ICTF-15) 012004. https://doi.org/10.1088/1742-6596/417/1/012004
25 Z. Wang and M. Wang: 3rd IEEE Eurasia Conf. IoT, Communication and Engineering (ECICE) (IEEE, 2021) 497–499. https://doi.org/10.1109/ECICE52819.2021.9645711
26 D. Beegan, S. Chowdhury, and M. T. Laugier: Surf. Coat. Tech. **201** (2007) 5804. https://doi.org/10.1016/j.surfcoat.2006.10.031
27 K. Wang, Z. Zheng, Y. Su, Z. Wang, L. Song, and J. Zhu: Opt. Express **17** (2009) 4468. https://doi.org/10.1364/OE.17.004468